Thin Solid Films 545 (2013) 424–428

Contents lists available at ScienceDirect

Thin Solid Films

journal homepage: www.elsevier.com/locate/tsf

Enhanced photovoltaic performance of inverted polymer solar cells by tuning the structures of titanium dioxide

Ruixiang Peng [a], Feng Yang [a], Xinhua Ouyang [a], Ying Liu [a], Yong-Sang Kim [b], Ziyi Ge [a,*]

[a] Ningbo Institute of Material Technology & Engineering, Chinese Academy of Sciences, Ningbo 315201, PR China
[b] Department of Electrical Engineering, Myongji University, Gyeonggi 449-728, South Korea

ARTICLE INFO

Article history:
Received 5 July 2012
Received in revised form 15 July 2013
Accepted 17 July 2013
Available online 24 July 2013

Keywords:
Titanium dioxide
Thin films
Inverted polymer solar cells
Photovoltaic performance

ABSTRACT

Inverted polymer solar cells using TiO_2 film as electron transporting layer were fabricated with the structure of fluorine-doped tin oxide/TiO_2 films/poly(3-hexylthiophene): [6,6]-phenyl-C_{61}-butyric acid methyl ester/Poly(3,4-ethylenedioxythiophene):poly(styrenesulfonate)/Ag. By tuning the crystalline structure of TiO_2 films, the photovoltaic performance of the devices was remarkably enhanced. TiO_2 was prepared by sol-gel method and their structures, morphologies and transmittance were characterized by X-ray diffraction, scanning electron microscope, and UV-visible spectrophotometer. Interestingly, for TiO_2-3 film, which was prepared with tetrabutyl titanate, acetyl acetone and ethanol in a ratio of 1:0.5:6, the open-circuit voltage and fill factor of the device were up to 0.6 V and 64.8%, respectively, and the power conversion efficiency of TiO_2-3 film was achieved up to 3.56% with the current density of 9.18 mA/cm^2 under an AM 1.5 G (100 mW/cm^2) irradiation intensity. In the meanwhile, the stabilities of these devices were also studied and results showed that our work was better than the corresponding devices of conventional structure.

1. Introduction

Bulk heterojunction solar cells have been attracting extensive research efforts in the past decades due to their advantages of lightweight, low cost and flexibility. The performance of laboratory-scale polymer solar cells based on different electron donor and acceptor materials have been remarkably improved, and some reports with power conversion efficiencies up to 7% at Air Mass 1.5 Global (AM 1.5G) has been demonstrated [1–3]. In these reports, the typical cells consist of a bottom indium tin oxide (ITO) anode, a Poly(3,4-ethylenedioxythiophene): poly(styrenesulfonate) (PEDOT:PSS) anode interfacial layer, a photoactive layer and a low-work-function top metal cathode. However, studies showed that PEDOT:PSS degraded the property of devices due to its corrosion of ITO [4]. In addition, the prolonged exposure of these kinds of devices to air can lead to oxidation of the electrode and degradation of the active layer from oxygen and moisture diffusion through grain boundaries and pinholes of the metal electrode without encapsulation, which will seriously limit their application [5,6]. In order to solve these problems, an approach was employed by inserting a metal oxide buffer layer between the active layer and ITO anode to reduce the amount of damage and oxygen diffusion into the polymer. Recently, different types of solution- processed sol-gel titanium oxide and zinc oxide have been used as buffer layer to overcome these problems and improve device stability in ambient conditions, these architectures are called "inverted cells" [7–11]. Nanocrystalline TiO_2 porous films are widely used for the dye-sensitized solar cells, this type of solar cells have achieved the overall efficiency of 10% and remarkable stability under simulated solar light [12,13], which is comparable to that of amorphous silicon solar cells. TiO_2 films also provide a promising alternative to the electron transporting layer because of their low work function, high electron mobility and optical transparency, as well as their ease of synthesis [14,15], Despite these advantages, power conversion efficiencies of most of the TiO_2 based inverted polymer solar cells with poly(3-hexylthiophene): [6,6]-phenyl-C_{61}-butyric acid methyl ester (P3HT:PCBM) as active layer were below 3% [7,16]. TiO_2 film plays a significant role to affect the performance of this type of solar cells, the major challenges in using TiO_2 as ETL include poor spatial distribution of the nanoparticles over a large area [17,18]. Accordingly, it is necessary to optimize TiO_2 films structure so as to realize high efficiency inverted polymer solar cells.

In order to deeply improve the power conversion efficiency (PCE) of inverted polymer solar cells (PSCs), we synthesized a series of crystalline TiO_2 films in this paper. Their structures and morphologies were characterized by X-ray diffraction (XRD) and Scanning electron microscopy (SEM). The transmittance of TiO_2 substrates were tested by UV-visible spectrophotometer (UV-vis). The inverted polymer solar cells using TiO_2 films as electron transporting layers were fabricated with the following architecture: Fluorine-doped tin oxide (FTO)/TiO_2/P3HT:PCBM/PEDOT:PSS/Ag. In addition, the relationship between

* Corresponding author. Tel./fax: +86 574 86680273.
E-mail address: geziyi@nimte.ac.cn (Z. Ge).

0040-6090/$ – see front matter.
http://dx.doi.org/10.1016/j.tsf.2013.07.041

the performance of the photovoltaic cells and TiO_2 thin film structures were demonstrated in the article.

2. Experimental details

2.1. Materials and the methods

Fluorine-doped tin oxide glass sheet (2.2 mm thick, ≤14 Ω/square, transmittance > 90%) was purchased from Nippon Sheet Glass Company, Ltd, PEDOT:PSS (Baytron® P VP Al 4083) and $PC_{60}BM$ were purchased from Luminescence Chemical Engineering Technology Co., Ltd, titanium tetraisopropoxide (Acros, 98 +%), titanium isopropoxide (Acros, 98 +%), tetrabutyl titanate (Acros, 98 +%), titanium ethoxide (Acros, 98 +%), dichlorobenzene and hexamethylene disilazane (HMDS) were purchased from Acros. All other reagents were obtained from Sinopham Chemical Reagent Co., Ltd, and used as received if not specified. P3HT was synthesized following the method described elsewhere [19], the average molecular mass (Mw) of the synthesized polymer was 32,000 with a polydispersity index of 1.6, as determined with a WATERS 150-C gel permeation chromatography (GPC) with THF as solvent and monodispersed polystyrene as standard.

2.2. Preparation of TiO_2 solutions

Four different kinds of TiO_2-sol were prepared and named TiO_2-1, TiO_2-2, TiO_2-3 and TiO_2-4.

TiO2-1 Titanium tetraisopropoxied, absolute ethanol, and acetic acid were mixed with the volume ratio of 1:20:0.1.The reaction was stirred at room temperature until a homogeneous colorless stable TiO_2-sol was obtained, which was assigned as TiO_2-1.

TiO2-2 Titanium isopropoxide ($C_{12}H_{28}O_4Ti$), isopropanol, hydrochloric acid (HCl, 0.28 mol/L), and distilled water were mixed with the volume ratio of 3:20:0.1:0.2. The reaction was stirred at room temperature until a yellowish color TiO_2-sol was formed and named as TiO_2-2.

TiO2-3 The preparation process was same with the TiO_2-1. We changed the Titanium tetraisopropoxied to tetrabutyl titanate ($Ti(OC_4H_9)_4$) and the ratio of 1:0.5:6 to $Ti(OC_4H_9)_4$, acetyl acetone and ethanol in the reaction. A stable yellow TiO_2-sol was synthesized and labeled as TiO_2-3.

TiO2-4 The preparation process was similar as above. TiO_2 was prepared by mixing titanium (IV) ethoxide, HCl (0.28 mol/L), and isopropyl alcohol with the ratio of 5:1:30, a light yellow stable TiO_2-sol was obtained and labeled as TiO_2-4.

2.3. Devices fabrication

A solution of P3HT and PCBM was prepared using 1,2-dichlorobenzene as solvent. The concentration of the solution was maintained around 35 mg/mL with 1% (v/v) 1,8-octanedithiol. The inverted polymer solar cells with the sandwich structure of FTO/TiO_2/P3HT: PCBM/PEDOT:PSS/Ag were fabricated. The above-prepared TiO_2-sol was spin-coated on a cleaned FTO substrates (2.54 cm × 2.54 cm), which were cleaned by a routine cleaning procedure which includes initial manual washed in aqueous detergent, and then sequentially sonication in acetone, isopropanol, and deionized water, lastly rinsing in ethanol and drying in a N_2 stream. The TiO_2 layer was sintered at 500 °C for 1 h under ambient conditions. The pre-dissolved composite solution was filtered through 0.45 μm syringe filter and then an active layer of about 300 nm was spin coated on the TiO_2 layer. Subsequently, hexamethyldisilazane (HMDS) was coated immediately onto the active layer. PEDOT:PSS mixed with 1% (v/v) of Triton X-100 ($C_{14}H_{22}O(C_2H_4O)n$) nonionic surfactant was spin-coated onto the surface of the active layer. Thermal preannealing was conducted at 120 °C for 30 min on a hot plate in a glovebox ($H_2O \leq 0.1$ ppm, $O_2 \leq 0.1$ ppm). Finally, a cathode (top electrode) of Ag was deposited onto the PEDOT:PSS layer in a thermal evaporator under a vacuum of 5×10^{-5} Pa. The effective area of single solar cells was 0.1257 cm^2. The device structure of FTO/TiO_2 films/P3HT: PCBM/PEDOT: PSS/Ag is shown in Fig. 1.

2.4. Characterization

The thickness of films was measured using surface profiler (Dektak 150). The transmittance spectra of FTO and TiO_2 films were recorded using a Lambda 950 spectrophotometer. The crystalline structures were characterized by XRD (D8 advance) with a 2θ from 15° to 80° by 0.02° s^{-1} steps operating at 40 kV accelerating voltage and 40 mA current using Cu K radiation source, the incident angle was kept constant at 0.5° throughout the experimentation. The surface morphology and pore distribution of the produced films were studied using SEM at 4.0 kV (FEI Quanta FEG 250). The current–voltage (I–V) characteristics of all the photovoltaic cells were measured under the simulated solar light (100 mW cm^{-2}; AM 1.5 G) provided by a Newport-Oriel® Sol3A 1000-W solar simulator and stored in Ar atmosphere without encapsulation. Electrical data were recorded using a Keithley 2440 source-measure unit, the intensity of the simulated solar light was calibrated by a standard Si photodiode detector (PV measurements Inc.), which was calibrated at National Renewable Energy Laboratory of the United-States. The external quantum efficiency (EQE) spectra were measured by a Newport-Oriel® IQE 200™ under illumination with monochromatic light from a Xe lamp at room temperature in Air atmosphere.

3. Results and discussion

Fig. 2 shows the surface micrographs of different TiO_2 films using SEM which were spin-coated on the FTO substrate and annealed at 500 °C. As shown in the figures, TiO_2-1 film (a) presented a smooth morphology in elongated domains, but in the edge area, the surface with many cracks was observed. For the substrate of TiO_2-2, the surface is inhomogeneously covered by large aggregates consisting of typically 5 μm dimension scales, the aggregates are separated by many cracks probably formed during the drying process due to surface tension between the film and the air [20]. The large aggregates in the matrix may limit the transformation from anatase to rutile phase, and the sintering process resulted in a low crystallite and a poor charge mobility of the film. In picture (c) TiO_2-3 films and (d) TiO_2-4 films, well-defined homogeneous surface morphologies with nanoparticle-shaped domains can be clearly seen. These equally distributed nanoparticles can offer more interface for charge separation and transmission between the inorganic TiO_2 composites and donor materials, which will be beneficial to enhance the performance of solar cells.

To reveal the deep information of the crystal nanoparticle's size and structure, TiO_2 films were studied by X-Ray Diffraction measurement, which can be used more quantitatively to study particle size and distribution of nanoparticles as well as other structure-related parameters

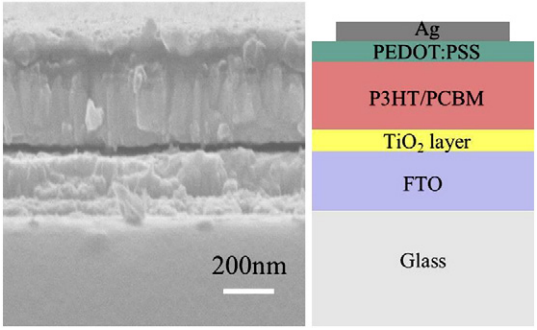

Fig. 1. SEM image of device cross section and schematic structure of the inverted polymer solar cells.

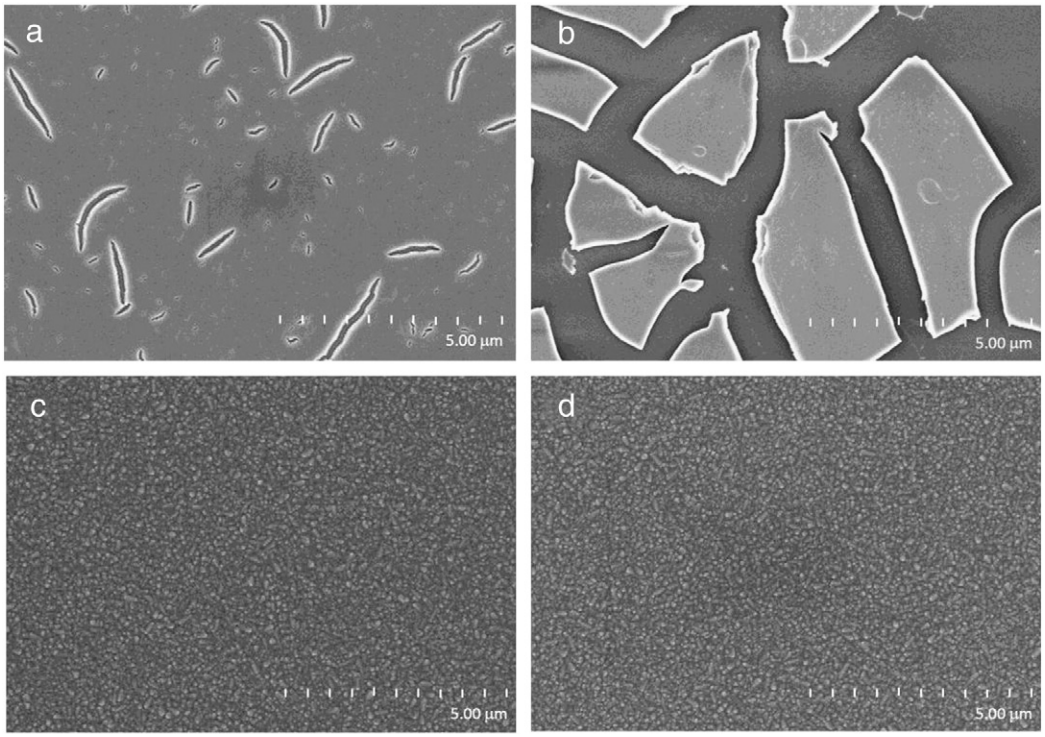

Fig. 2. SEM micrographs of the surface of varied TiO_2 films spin-coated on the FTO substrate after annealing at 500 °C, corresponding to (a) TiO_2-1, (b) TiO_2-2,(c) TiO_2-3, (d) TiO_2-4, respectively.

[21]. The XRD patterns of as-prepared TiO_2 films are shown in Fig. 3. The 2θ value of the (101) peak for anatase and rutile are at around 25.0° and 26.5°, respectively. The mark * denotes the FTO substrates reflection peak.

By analyzing the XRD results of the TiO_2 films sintered at 500 °C for 1 h, it can be proved that both anatase and rutile structures exits in the TiO_2-2, and the rutile phase is the major component. The angular dispersion of a diffraction peak (FWHM) provides dimensional information of the crystalline region that is responsible for the scattering X-rays, and the crystallite size (S) can be calculated from the full width at half maximum of the (101) peak for anatase or rutile by Debye-Scherer formula in Eq. (1). $S = 0.9\lambda(B\cos(\theta))^{-1}$. where λ is the wavelength of the X-rays used (λ = 0.14 nm), B is the FWHM (radians), and θ is the Bragg angle of peak (degree). The detailed analysis is summarized in Table 1. As clearly shown in Fig. 3, crystal size from ca. 25.8 nm to 53.5 nm appeared in the as-prepared TiO_2 films, which is comparable to the data of SEM images.

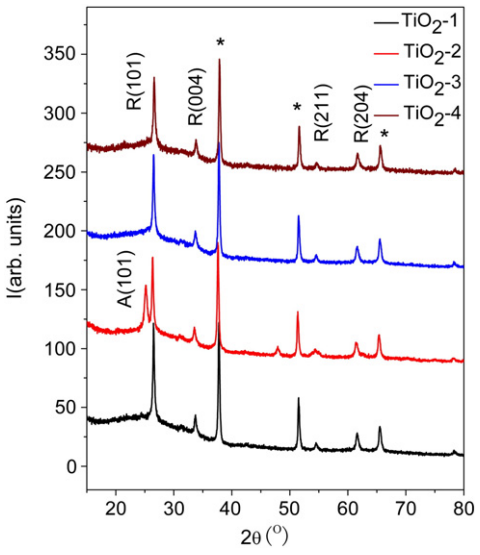

Fig. 3. X-Ray diffraction patterns of the as-prepared TiO_2 thin films spin-coated on the FTO substrate after annealing at 500 °C. The mark * donates the FTO substrate reflection peak.

For the TiO_2-1 film, the minimum crystal size is around ca. 25.8 nm, while the TiO_2-3 film showed the maximum crystal size around ca. 53.5 nm. For the TiO_2-3 and TiO_2-4, the crystal sizes are almost the same, but the relative crystallite for TiO_2-3 is 0.92, which is much higher than that of TiO_2-4 (0.86). The values were calculated by $I_{A(101)}/I_{FTO}$ according to the comparative value of the FTO substrate reflection peak at around 37.0°. The higher crystallite of TiO_2-3 film should be beneficial for improving electron mobility resulting in an overall enhanced performance of the PSCs.

The transmittances of FTO and TiO_2 films spin-coated on the FTO glass substrate were investigated by UV-visible spectrophotometer after sintering at 500 °C for 1 h. The measurement technique for all the samples was same. The transmittance of FTO was reduced to 80% after sintering compared to the initial value, which is mainly caused by the high resistance of the FTO layer after it was annealed at high temperature [22]. Moreover, after spin-coating the TiO_2 layer on the FTO substrate, different degrees of transmittance ranging from 400 to 700 nm was found which corresponds to the main absorption region of P3HT. As far as TiO_2-1 film was considered, the transmittance of TiO_2-1 film was

Table 1
Detailed information derived from the XRD analysis (Note: (a) A and R corresponds to the anatase and rutile structure of the TiO_2 films, respectively. (b) Crystallite size was calculated using the FWHM values according to the equation of $S = K\lambda(B\cos\theta)^{-1}$).

Samples	2θ (deg)	FWHM (deg)	S (nm)	$I_{A(101)}/I_{FTO}$
TiO_2-1	26.5	0.280	25.8	0.98
TiO_2-2	25.0^A	0.261	27.8	–
	26.3^R	0.160	45.2	0.91
TiO_2-3	26.5	0.135	53.5	0.92
TiO_2-4	26.5	0.147	49.2	0.86

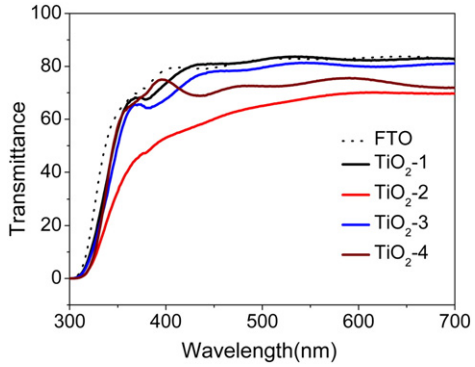

Fig. 4. The transmittance spectra of FTO substrate and as-prepared TiO_2 films.

almost the same with the FTO substrate at the region of visible light. Actually, an absolute rutile structure and a high crystallite formed in this TiO_2 film lead to a high transmittance, which had been confirmed by the XRD analysis. The TiO_2-2 film has the lowest transmittance due to the excitation of the anatase structures in the samples after sintering at 500 °C. Additionally, large aggregates in the matrix were also observed in the SEM images which lead to a poor light transmittance. As shown in Fig. 4, the transmittance of TiO_2-3 film was higher in comparison with that of TiO_2-4 in the range of 400 to700 nm. The optical and crystal characteristics of TiO_2 films have an important influence on the incident light absorption, high transmittance of the TiO_2 film was beneficial for improving the absorption efficiency of PCBM:P3HT active layer, consequently resulting in increased total exciton number leading to a higher short circuit current [23,24].

The influence of TiO_2 layer on the inverted PSCs performance with a structure of FTO/TiO_2 films/P3HT:PCBM/PEDOT:PSS/Ag were investigated. The J–V curves characterized under AM 1.5 with an irradiation intensity of 100 mW/cm^2 are shown in Fig. 5(a), some important parameters of photovoltaic performance are summarized in Table 2. The device performance with optimized TiO_2-3 film exhibited the highest power conversion efficiency of 3.56%, with the short-circuit current (J_{SC}) = 9.18 mA/cm^2, open-circuit voltage (V_{OC}) = 0.6, and fill factor (FF) = 64.8%. While PCE of TiO_2-4 film was 3.23% with J_{SC} = 9.28 mA/cm^2, V_{OC} = 0.6, and FF = 58.1%. For TiO_2-1 film solar cells, the PCE was only 1.90% with J_{SC} = 11.0 mA/cm^2, V_{OC} = 0.42, and FF = 40.9%. Correspondingly, solar cell with TiO_2-2 film shows a PCE of 1.05%, J_{SC} = 6.80 mA/cm^2, V_{OC} = 0.50, and FF = 30.2%. It can be seen that the power conversion efficiency is critically sensitive to the TiO_2 film structure. TiO_2-1 film devices exhibited a highest J_{SC} of 11.0 mA/cm^2, the improved J_{SC} were mainly caused by the higher crystallite (Fig. 3) and transmittance (Fig. 4) of the synthesized TiO_2 film. However, the values of V_{OC} and FF were dramatically decreased due to the surface morphology defects of TiO_2 films, the interfacial area between the smooth TiO_2-1 film and the P3HT:PCBM active layer is lower, leading to a low exciton dissociation efficiency. In the meanwhile, large aggregate morphology of TiO_2-2 film will resulted in serious charge recombination [23,24]. According to the literature the Voc is determined by the differences between the highest unoccupied molecular orbital energy of the donor and lowest unoccupied molecular orbital energy of the fullerene acceptor [25], but it has been reported that the Voc is also determined by recombination at the donor/acceptor interface [26,27].

The optimized TiO_2-3 films and TiO_2-4 films with well-defined homogeneous nanoparticle-shaped domain morphologies provides more interface and pathway for exciton dissociation and charge separation, thereby improving the performance of the solar cells, especially TiO_2-3 film solar cells exhibited a FF = 64.8% and a highest PCE of 3.56%, which means low charge recombination and more photo-induced carriers can transport to the correct electrode.

Fig. 5(b) shows the J–V characterization under dark condition, the gradient of curves reflect the series resistance of the solar cells [28], TiO_2-2 device exhibited a resistance of 299.8 Ω/cm^2, much higher than that of TiO_2-3 device with a value of 71.8 Ω/cm^2, the high resistance leads to a reduced FF and J_{SC}, then limiting the PCE of TiO_2-2

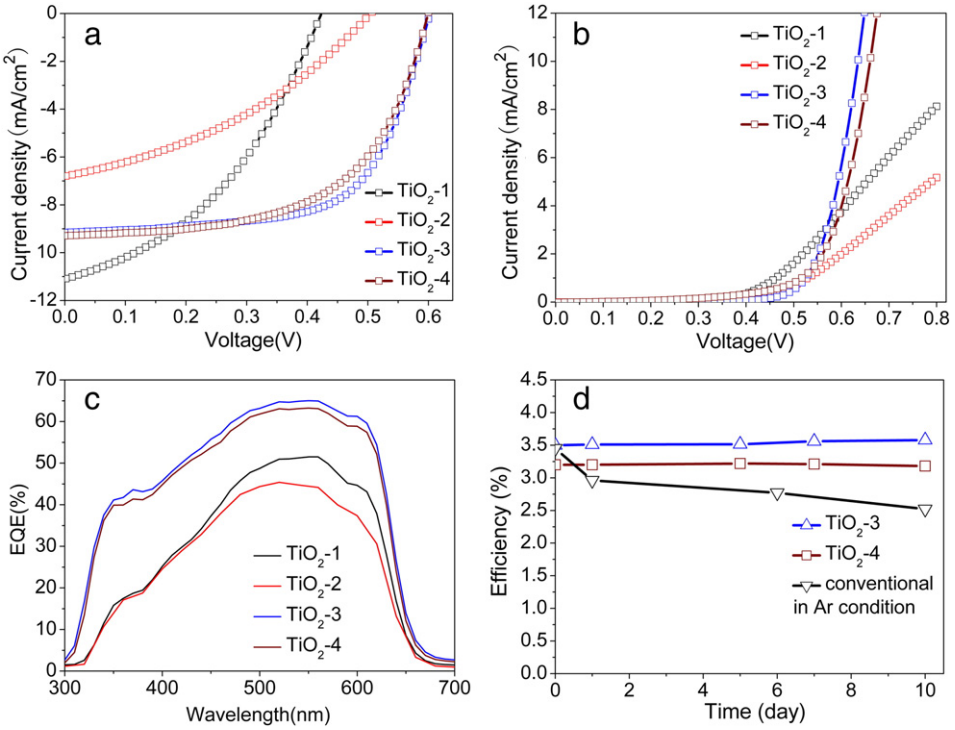

Fig. 5. J–V characteristics of the inverted polymer solar cells prepared by different TiO_2 films at (a) an irradiation intensity of 100 mW/cm^2 and (b) dark condition, (c) the EQE spectra of devices, (d) the performance stabilities of the devices in argon atmosphere over a period of 10 days.

Table 2
Photovoltaic performance of polymer solar cells fabricated using varied TiO_2 films, which were measured under AM 1.5 with an irradiation intensity of 100 mW/cm^2.

samples	V_{OC} (V)	J_{SC} (mA/cm^2)	*FF* (%)	$R_{at\ VOC}$ (Ω)	PCE(%)
TiO_2-1	0.42	11.0	40.9	131.8	1.90
TiO_2-2	0.50	6.80	30.2	299.8	1.05
TiO_2-3	0.60	9.18	64.8	71.8	3.56
TiO_2-4	0.60	9.28	58.1	82.1	3.23

solar cells which is about 30 percent of that of TiO_2-3 devices. The external quantum efficiencies (EQE) of the devices are shown in Fig. 5(c), the EQE values up to 65% for TiO_2-3 devices is higher than other's in most of the spectral region, especially in the range from 300 to 400 nm, the EQE values of TiO_2-1 and TiO_2-2 devices is much lower than that of TiO_2-3 and TiO_2-4, that maybe caused by the incomplete charge carrier collection efficiencies. In addition, a durability test of these devices was performed under argon atmosphere without encapsulation. The PCEs with respect to exposure time for TiO_2-3 and TiO_2-4 are shown in Fig. 5(d). For comparison with the conventional structure of solar cells, we also fabricated a device with ITO/PEDOT:PSS/P3HT/P3HT:PCBM/LiF/Al structure. Obviously, the inverted solar cells exhibited excellent stability under argon atmosphere, their PCE remained almost the same as the original value after 10 days, while the PCE of conventional devices decreased to about 70% of the original value. The results are in agreement with the reports of this kind of devices under ambient conditions [9–11]. The inverted solar cells with TiO_2 layers also present an excellent stability performance in air atmospheres; the stability mechanism of the devices in air atmospheres were carefully investigated by another report [29], devices exhibited only 5% decay of the power conversion efficiency while being exposed in air atmospheres without encapsulation for more than 20 days. Actually, in the conventional solar cells, the rapid PCE decay is mainly caused by the infiltration of moisture to the active layer. Correspondingly, the inverted cells with TiO_2 layers were air stable due to protection for the active materials of TiO_2 films.

4. Conclusions

In conclusion, we synthesized a series of crystalline TiO_2 thin films with different structures by sol-gel method and used them as electron transporting layers. Inverted polymer solar cells with FTO/TiO_2/P3HT:PCBM/PEDOT:PSS/Ag structure were fabricated by optimizing TiO_2 films. Interestingly, the device with TiO_2-3 exhibited a high power conversion efficiency up to 3.56% under an AM 1.5 G (100 mW/cm^2) irradiation intensity. The values of J_{SC}, V_{OC} and FF were 9.18 mA/cm^2, 0.6 V, and 64.8%, respectively. The results showed that well-defined and homogeneous morphology of TiO_2 films was beneficial for exciton dissociation and charge separation. Furthermore, the devices with TiO_2-3 and TiO_2-4 film present excellent stabilities in Ar condition after 10 days. Our work paves a way to improve the performance of the inverted PSCs, in particular, for PCE, FF and stability of inverted polymer solar cells.

Acknowledgements

This work was financially supported by the National Natural Science Foundation of China (21074144), The Fok Ying-Tong Education Foundation (122027), The NIMTE Foundation (Y20841QF07), Qianjiang Telent Project, and visiting professorship for Senior International Scientists from Chinese Academy of Science.

References

[1] Y.Y. Liang, L.P. Yu, Acc. Chem. Res. 43 (2010) 1227.
[2] H.-Y. Chen, J.H. Hou, S.Q. Zhang, Y.Y. Liang, G.W. Yang, Y. Yang, L.P. Yu, Y. Wu, G. Li, Nat. Photonics 3 (2009) 649.
[3] C.E. Small, S. Chen, J. Subbiah, C.M. Amb, S.W. Tsang, T.H. Lai, J.R. Reynolds, F. So, Nat. Photonics 6 (2011) 115.
[4] J. Subbiah, C.M. Amb, I. Irfan, Y.L. Gao, J.R. Reynolds, F. So, ACS Appl. Mater. Interfaces 4 (2012) 866.
[5] K. Norrman, M.V. Madsen, S.A. Gevorgyan, F.C. Krebs, J. Am. Chem. Soc. 132 (2010) 16883.
[6] K. Norrman, S.A. Gevorgyan, F.C. Krebs, ACS Appl. Mater. Interfaces 1 (2009) 102.
[7] H. Schmidt, H. Flügge, T. Winkler, T. Bülow, T. Riedl, W. Kowalsky, Appl. Phys. Lett. 94 (2009) 243302.
[8] W.H. Baek, M.J. Choi, T.S. Yoon, H.H. Lee, Y.S. Kim, Appl. Phys. Lett. 96 (2010) 133506.
[9] J.H. Huang, H.Y. Wei, K.C. Huang, C.L. Chen, R.R. Wang, F.C. Chen, K.C. Ho, C.W. Chu, Energy Environ. Sci. 3 (2010) 654.
[10] S.K. Hau, H.L. Yip, N.S. Baek, J. Zou, K.O. Malley, A.K.Y. Jen, Appl. Phys. Lett. 92 (2008) 253301.
[11] K. Lee, J.Y. Kim, S.H. Park, S.H. Kim, S. Cho, A.J. Heeger, Adv. Mater. 19 (2007) 2445.
[12] S. Ito, S.M. Zakeeruddin, R. Humphry-Baker, P. Liska, R. Charvet, P. Comte, M.K. Nazeeruddin, P. Péchy, M. Takata, H. Miura, S. Uchida, M. Grätzel, Adv. Mater. 18 (2006) 1202.
[13] Y. Bai, Y.M. Cao, J. Zhang, M.K. Wang, R.Z. Li, P. Wang, S.M. Zakeeruddin, M. Grätzel, Nat. Mater. 7 (2008) 626.
[14] H.W. Geng, M.T. Wang, S.K. Han, R.X. Peng, Sol. Energy Mater. Sol. Cells 94 (2010) 547.
[15] C.H. Wu, H.Y. Li, H.H. Fong, V.A. Pozdin, L.A. Estroff, G.G. Malliaras, Org. Electron. 12 (2011) 1073.
[16] C. Tao, S.P. Ruan, X.D. Zhang, G.H. Xie, L. Shen, Appl. Phys. Lett. 93 (2008) 193307.
[17] S. Monticone, R. Tufeu, A.V. Kanaev, J. Phys. Chem. B 102 (1998) 2854.
[18] S. Sakohara, M. Ishida, M.A. Anderson, J. Phys. Chem. B 102 (1998) 10169.
[19] J.P. Lamps, J.M. Catala, Macromolecules 44 (2011) 7962.
[20] A. Elfanaoui, E. Elhamri, L. Boulkaddat, A. Ihlal, K. Bouabid, L. Laanab, A. Taleb, X. Portier, Int. J. Hydrog. Energy 36 (2011) 4130.
[21] N.C. Das, P.E. Sokol, Renew. Energy 35 (2010) 2683.
[22] T. Kawashima, T. Ezure, K. Okada, H. Matsui, K. Goto, N. Tanabe, J. Photoch, J. Photochem. Photobiol. A Chem. 164 (2004) 199.
[23] B. Juan, G.B. Germà, J. Phys. Chem. Lett. 2 (2011) 1950.
[24] K. Vandewal, K. Tvingstedt, A. Gadisa, O. Inganäs, J.V. Manca, Nat. Mater. 8 (2009) 904.
[25] C.J. Brabec, A. Cravino, D. Meissner, N.S. Sariciftci, T. Fromherz, M.T. Rispens, L. Sanchez, J.C. Hummelen, Adv. Funct. Mater. 11 (2001) 374.
[26] J. Nelson, J. Kirkpatrick, P. Ravirajan, Phys. Rev. B 69 (2004) 035337.
[27] T. Kirchartz, J. Mattheis, U. Rau, Phys. Rev. B 78 (2008) 235320.
[28] C.H. Chou, W.L. Kwan, Z. Hong, L.M. Chen, Y. Yang, Adv. Mater. 22 (2010) 1.
[29] R. Peng, F. Yang, X. Ouyang, Y. Liu, Y. Kim, Z. Ge, Appl. Phys. A (2013), http://dx.doi.org/10.1007/s00339-013- 7626-2.